Water Supply

IWA PUBLISHING

Water Supply Vol 22 No 1, 31 doi: 10.2166/ws.2021.288

An analytical model for vortex at vertical intakes

Hamed Sarkardeh[a,*] and Morteza Marosi[b]

[a] Department of Civil Engineering, Faculty of Engineering, Hakim Sabzevari University, Sabzevar, Iran
[b] Hydraulic Structures Division, Water Research Institute, Tehran, Iran
*Corresponding author. E-mail: sarkardeh@hsu.ac.ir

ABSTRACT

In the present paper, free surface vortex formation at intakes is investigated analytically. By assuming a spiral form for vortex streamlines, continuity and momentum equations were integrated and solved in a vortex flow domain. From this solution, velocity and pressure distributions were found above the intake under vortex action. An equation for the water surface profile was also found and compared with another research. By considering that in an air core vortex, pressure at the intake entrance drops to zero, a relationship was found for critical submerged depth and verified by experimental data and another analytical equation. It was concluded that the results of the proposed spiral analytical model had good agreement with the experimental data.

Key words: critical submerged depth, free surface, Navier-Stokes equations, pressure and velocity distributions, spiral vortex flow

HIGHLIGHTS

- Analytical analysis of free surface vortex phenomenon over a vertical intake in the reservoir.
- Solving 3D Navier-Stokes equations analytically for a swirling flow.
- Predicting the critical submergence at a vertical intake.
- Extracting pressures and velocities analytically using spiral theory.
- Comparing obtained analytical results with previous experimental and analytical results.

NOTATIONS

The following symbols are used in this paper:

D	intake pipe diameter
Fr	intake Froude Number $= V/\sqrt{gD}$
Γ	vortex strength
N_Γ	circulation number
g	gravitational acceleration
g_r	gravitational acceleration in r direction
g_z	gravitational acceleration in z direction
g_θ	gravitational acceleration in θ direction
Re	intake Reynolds number $= VD/\vartheta$
S	intake submerged depth
S_c	critical intake submerged depth
V	intake flow velocity
ϑ	kinematic viscosity
ρ	density of water
σ	surface tension of water
r, θ and z	coordinate directions
r	distance from the vortex center
r_m	radius at the maximum tangential velocity
V_θ	tangential velocity
V_r	radial velocity
V_z	velocity in the z direction
P	pressure
ω	Angular velocity

INTRODUCTION

Vortices are often experienced in nature and industries; for example in the course of water withdrawing at intakes (Khanarmuei *et al.* 2016; Khadem Rabe *et al.* 2018; Tahershamsi *et al.* 2018; Pakdel *et al.* 2020) and may be important for the desalination and treatment of saline wastewater (Panagopoulos *et al.* 2019; Panagopoulos & Haralambous 2020; Panagopoulos 2021). In spite of their common occurrence, vortex structure, formation and dynamics, are still not completely understood (Stepanyants & Yeoh 2008). Many factors affect on vortex formation and flow field near the intake structure such as asymmetry in the inflow and reservoir geometry (Roshan *et al.* 2009; Amiri *et al.* 2011; Sarkardeh *et al.* 2012; Sarkardeh *et al.* 2013), flow velocity in the intake, submerged depth and diameter of the intake pipe. Study of free surface vortices is important and necessary not only from a purely academic view, but also for a better understanding of such fluid phenomena in practical engineering systems. Most vortices in nature, however, have a 'spatial' structure; that is, the streamlines are not perpendicular to the axis of rotation (Lugt 1983). There are visual evidences as well as computational simulations that show the vortex streamlines follow a spiral path (Lugt 1983; Shukla & Kshirsagar 2008; Lucino *et al.* 2010; Sarkardeh *et al.* 2014). A schematic and real spiral vortex are presented in Figure 1(a) and 1(b) respectively.

One important case in engineering practice is withdrawing water at intakes. Surface vortex formation at intakes is an undesirable phenomenon, causing air entrainment into the intake, vibration and energy loss (Knauss 1987). Vortices can be divided into six types based on visual classification at the Alden Research Laboratory (Padmanabhan & Hecker 1984). Type 1 is observed as a weak rotation of flow at the water surface. In Type 2, in addition to water surface rotation, a dimple is also observed at the water surface. In Type 3, the rotation of the flow extends down to the intake itself. In Type 4, debris is dragged into the intake. In Type 5, some air bubbles are entrained from the water surface and are transported down to the intake. In the strongest surface vortex (Type 6), a stable air core is formed in the center of the vortex and air is steadily entrained into the tunnel (Knauss 1987). To prevent air entrainment of surface vortices, a minimum submerged depth of the intake, called the critical submerged depth S_c, is recommended for the intake (Figure 2(a)). Submerged depth is defined as the vertical distance between the water surface and the level of the intake center (Figure 2(b)).

Vortex phenomenon is studied with three different possible approaches: i-experimentally, ii-numerically and iii-analytically. In the experimental studies, a physical model has been constructed so that the scale effects were minimized. Vortices were then studied in different hydraulic and geometric conditions and related hydraulic factors were measured. By collecting data, empirical equations have been developed and proposed for practical hydraulic designs such as for critical submerged depth (Denny & Young 1957; Berge 1966; Gordon 1970; Reddy & Pickford 1972; Amphlett 1976; Chang 1977; Anwar *et al.* 1978; Jain *et al.* 1978; Sarkardeh *et al.* 2010; Amiri *et al.* 2011). In numerical studies, by discretizing governing equations, flow motion equations have been solved for the flow domain. Results also have been verified by experimental data. The results of this approach could help future simulations and prevent extra costs in physical modeling (Constantinescu & Patel 1998, 2000; Marghzar *et al.* 2003; Shukla & Kshirsagar 2008; Lucino *et al.* 2010; Sarkardeh *et al.* 2014). There have been also several attempts at analytical solution of vortex at intakes (Rott 1958; Lundgren 1985; Miles 1998; Andersen *et al.* 2003, 2006; Lautrup 2005; Stepanyants & Yeoh 2008; Yildirim *et al.* 2012; Schneider *et al.* 2015).

Maybe the first analytical study on vortex was done by Rankine (1858). He suggested a simple model for analyzing an intake vortex. In his proposed model the inner core is assumed as a forced and the outer region as a free vortex. The boundary

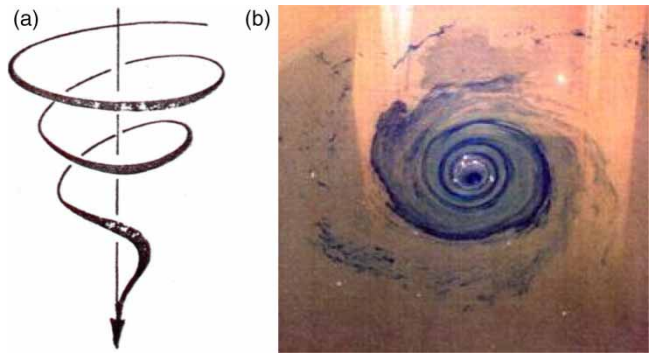

Figure 1 | Spiral streamlines in a vortex (a) from Lugt (1983) and (b) from WRI (1992).

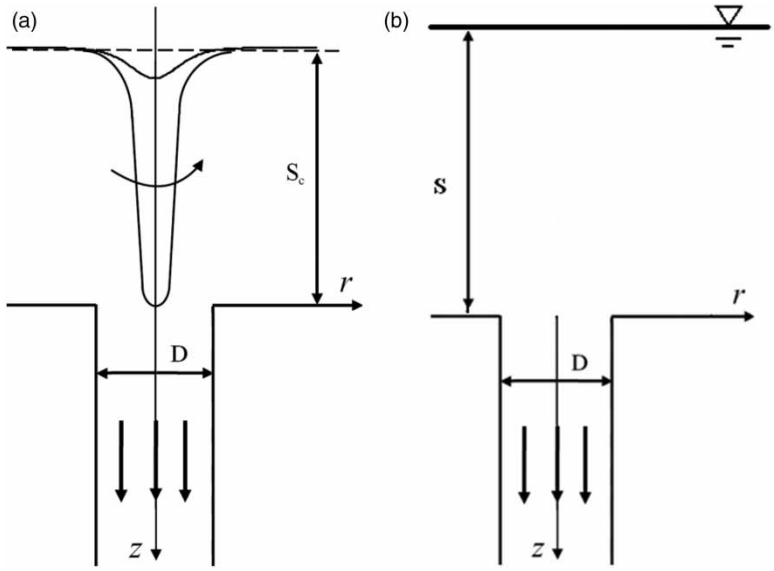

Figure 2 | Schematic view of an intake and parameter definitions (a) with an air core vortex (b) without vortex.

between the forced inner and irrotational outer free vortex is located at a distance equal to the radius of the intake from the axis of rotation. In the Rankine (1858) Model the velocity component in z direction is ignored and streamlines are considered as concentric circles. Rankine (1858) also defined vortex strength by its circulation as (White 2003):

$$\Gamma_{\text{at free vortex region}} = 2\pi r V_\theta \tag{1}$$

$$\Gamma_{\text{at forced vortex region}} = 2\pi r^2 \omega \tag{2}$$

where Γ is vortex strength, ω is angular velocity and V_θ is the tangential velocity at a distance r from the vortex axis. It is obvious that Γ is constant in the irrotational part of the vortex and ω is constant in the forced part of the vortex.

Another analytical attempt to describe the vortex phenomenon and calculate the critical submerged depth was made by Odgaard (1986). He suggested a model which provided a reasonable relationship between the critical submerged depth (S_c see in Figure 2(a)) and flow parameters such as discharge, circulation, viscosity and surface tension. Odgaard (1986) model was based on exact solution of governing equations for viscous unbounded fluid. Odgaard (1986) assumed the flow situation as steady, axi-symmetric, incompressible and the radial velocity component nearly linear near the pipe entrance. He also, by integrating equations of motion and Navier-Stokes, developed the following equation without the surface tension term for calculating critical submerged depth:

$$\left(\frac{S}{D}\right)_{cr} = 0.074\frac{\Gamma}{\sqrt{gD^3}}\sqrt{Re} \tag{3}$$

Many simplifying assumptions were made to derive Odgaard (1986) equations.

In the present paper, by applying spiral form for vortex streamlines in continuity and momentum equations, governing equations in complete form were integrated and 3D flow domain was solved in the presence of an air core vortex. The critical submerged depth was then determined by implementing independent non-dimensional parameters. Moreover, the water surface and formed air core were plotted regarding the extracted equations from the spiral analytical model. Finally, proposed equations were compared with other researcher results.

THEORY AND GOVERNING EQUATIONS

The governing continuity and Navier–Stokes equations describing flow in a steady state incompressible fluid are given by the following set of equations (White 2003):

$$\frac{\partial V_r}{\partial r}+\frac{V_r}{r}+\frac{\partial V_z}{\partial z}+\frac{1}{r}\frac{\partial V_\theta}{\partial \theta}=0 \tag{4}$$

$$V_r\frac{\partial V_r}{\partial r}+\frac{V_\theta}{r}\frac{\partial V_r}{\partial \theta}-\frac{V_\theta^2}{r}+V_z\frac{\partial V_r}{\partial z}=-\frac{1}{\rho}\frac{\partial P}{\partial r}+g_r+\vartheta\left(\frac{\partial^2 V_r}{\partial r^2}+\frac{1}{r}\frac{\partial V_r}{\partial r}-\frac{V_r}{r^2}+\frac{1}{r^2}\frac{\partial^2 V_r}{\partial \theta^2}-\frac{2}{r^2}\frac{\partial V_\theta}{\partial \theta}+\frac{\partial^2 V_r}{\partial z^2}\right) \tag{5}$$

$$V_r\frac{\partial V_\theta}{\partial r}+\frac{V_\theta}{r}\frac{\partial V_\theta}{\partial \theta}+\frac{V_r V_\theta}{r}+V_z\frac{\partial V_\theta}{\partial z}=-\frac{1}{\rho}\frac{1}{r}\frac{\partial P}{\partial \theta}+g_\theta+\vartheta\left(\frac{\partial^2 V_\theta}{\partial r^2}+\frac{1}{r}\frac{\partial V_\theta}{\partial r}-\frac{V_\theta}{r^2}+\frac{1}{r^2}\frac{\partial^2 V_\theta}{\partial \theta^2}+\frac{2}{r^2}\frac{\partial V_r}{\partial \theta}+\frac{\partial^2 V_\theta}{\partial z^2}\right) \tag{6}$$

$$V_r\frac{\partial V_z}{\partial r}+V_z\frac{\partial V_z}{\partial z}+\frac{V_\theta}{r}\frac{\partial V_z}{\partial \theta}=-\frac{1}{\rho}\frac{\partial P}{\partial z}+g_z+\vartheta\left(\frac{\partial^2 V_z}{\partial r^2}+\frac{1}{r}\frac{\partial V_z}{\partial r}+\frac{1}{r^2}\frac{\partial^2 V_z}{\partial \theta^2}+\frac{\partial^2 V_z}{\partial z^2}\right) \tag{7}$$

where V_r, V_z and V_θ are the radial, axial and tangential components of the velocity field; g is the acceleration due to the gravity; ρ is the fluid density; p is the pressure; and ϑ is the kinematic viscosity. A spiral path in space in cylindrical coordinate scan be described by the following equations:

$$z=\frac{b}{c}\theta \tag{8}$$

$$r=\frac{a}{c}\theta \tag{9}$$

$$r=\frac{a}{b}z \tag{10}$$

where a, b and c are the controller coefficients to produce different spiral curves. Few spirals are plotted in Figure 3 using Equations (8)–(10).

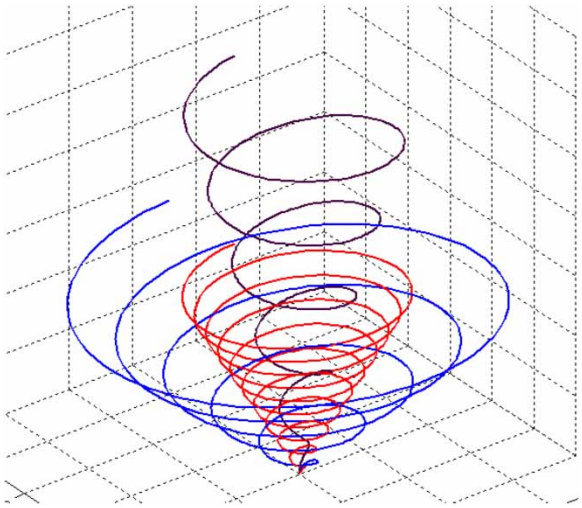

Figure 3 | Typical spiral curves using Equations (8)–(10).

By differentiating Equations (8)–(10) and using $V_r = dr/dt$, $V_z = dz/dt$, $V_\theta = rd\theta/dt$ flow velocity components can be written as:

$$V_r = \frac{a}{b} V_z \tag{11}$$

$$V_z = \frac{b}{c}\frac{1}{r} V_\theta \tag{12}$$

$$V_r = \frac{a}{c}\frac{1}{r} V_\theta \tag{13}$$

Along the streamlines one can write (Li & Lam 1964):

$$\frac{V_z}{V_r} = \frac{dz}{dr} \tag{14}$$

$$\frac{V_r}{V_\theta} = \frac{dr}{rd\theta} \tag{15}$$

$$\frac{V_\theta}{rd\theta} = \frac{V_z}{dz} \tag{16}$$

Substituting Equations (11)–(13) into Equations (14)–(16) confirms their correct expressions for velocity components. In addition the relationship found between velocity components in a spiral path (Equations (11)–(13)), satisfy the continuity Equation (4) too.

Free vortex region

Applying Equation (1) in Equations (11)–(13), and using Equations (8)–(10), tangential, axial and radial velocity components can be written as:

$$V_\theta = \frac{\Gamma}{2\pi r} \tag{17}$$

$$V_z = \frac{z\Gamma}{2\pi\theta r^2} \tag{18}$$

$$V_r = \frac{\Gamma}{2\pi\theta r} \tag{19}$$

One can plot spiral streamlines and velocity vectors from Equations (17) to (19) (Figure 4). For example by assuming $\Gamma = 0.4$ and θ between zero and 2π, three streamlines are plotted in Figure 4(a). 2D plot of these streamlines in xy plane is shown in Figure 4(b) and vector plot of xy component of velocity vector is also plotted in Figure 4(c).

Integrating navier-stokes equations for pressure distribution at free vortex region:

The origin of the cylindrical coordinate system (r, z, θ) was considered at the reservoir surface, and the z-axis directed downwards (Figure 2). Substituting Equations (17)–(19) in Equations (5)–(7) and integrating them yields:

In r direction:

$$\frac{\partial \mathrm{P}}{\partial \mathrm{r}} = \frac{\rho\Gamma^2}{4\pi^2 r^3} + \frac{3\rho a^2\Gamma^2}{2\pi^2 c^2 r^5} + \vartheta\left(\frac{5\rho a\Gamma}{2\pi c r^4} + \frac{3\rho a^3\Gamma}{\pi c^3 \mathrm{r}^6} + \frac{3\rho a^3\Gamma}{\pi c b^2 r^4}\right) \tag{20}$$

$$\mathrm{P_r} = -\frac{\rho\Gamma^2}{8\pi^2 r^2} - \frac{3\rho a^2\Gamma^2}{8\pi^2 c^2 r^4} - \vartheta\left(\frac{5\rho a\Gamma}{6\pi c r^3} + \frac{3\rho a^3\Gamma}{5\pi c^3 \mathrm{r}^5} + \frac{\rho a^3\Gamma}{\pi c b^2 r^3}\right) + C_1 \tag{21}$$

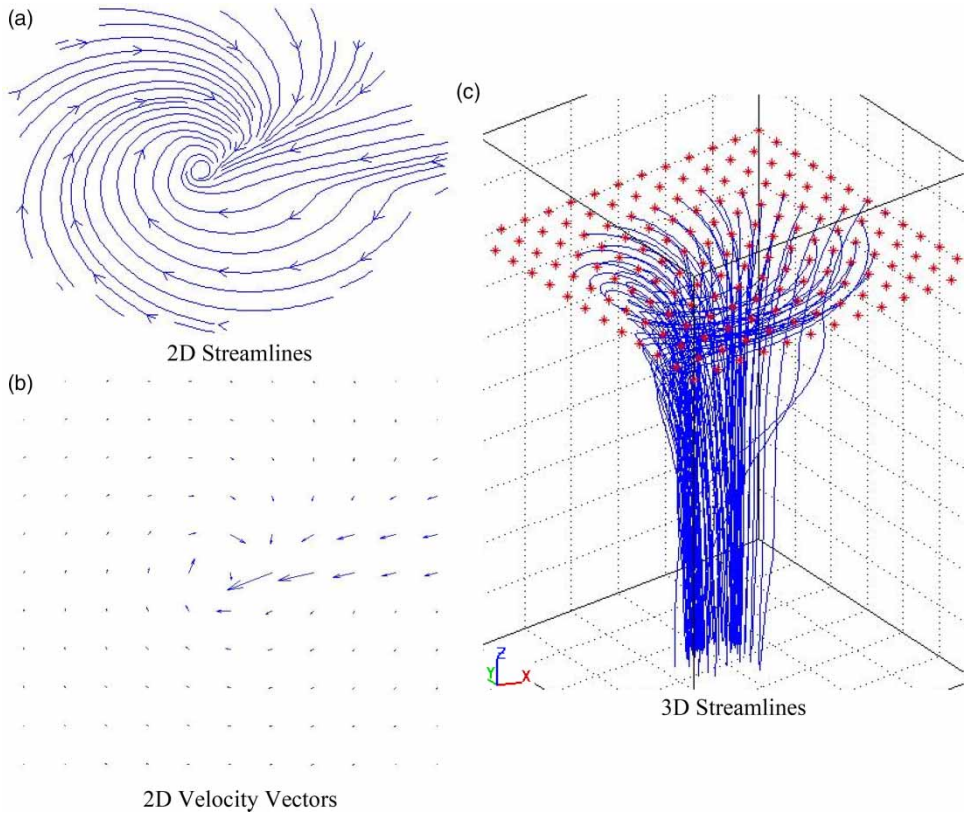

Figure 4 | Typical spiral streamlines and velocity vectors using Equations (17)–(19). (a) 2D streamlines. (b) 2D Velocity Vectors. (c) 3D Streamlines.

In θ direction:

$$\frac{\partial \mathrm{P}}{\partial \theta} = \frac{\rho c^2 \Gamma^2}{2\pi^2 a^2 \theta^3} + \vartheta\left(-\frac{\rho c^2 \Gamma}{a^2 \pi \theta^4} + \frac{\rho c^2 \Gamma}{\pi b^2 \theta^2}\right) \tag{22}$$

$$\mathrm{P}_\theta = -\frac{\rho c^2 \Gamma^2}{\pi^2 a^2 \theta^2} + \vartheta\left(\frac{3\rho c^2 \Gamma}{a^2 \pi \theta^3} - \frac{\rho c^2 \Gamma}{\pi b^2 \theta}\right) + C_2 \tag{23}$$

In z direction:

$$\frac{\partial \mathrm{P}}{\partial \mathrm{z}} = \frac{3\rho b^6 \Gamma^2}{2\pi^2 c^2 a^4 z^5} + \rho \mathrm{g} + \vartheta\left(\frac{2\rho b^5 \Gamma}{\pi c a^4 z^4} + \frac{3\rho b^7 \Gamma}{\pi a^4 c^3 \mathrm{z}^6} + \frac{3\rho b^3 \Gamma}{\pi c a^2 z^4}\right) \tag{24}$$

$$\mathrm{P}_\mathrm{z} = -\frac{3\rho b^6 \Gamma^2}{8\pi^2 c^2 a^4 z^4} + \rho \mathrm{gz} - \vartheta\left(\frac{2\rho b^5 \Gamma}{3\pi c a^4 z^3} + \frac{3\rho b^7 \Gamma}{5\pi a^4 c^3 \mathrm{z}^5} + \frac{\rho b^3 \Gamma}{\pi c a^2 z^3}\right) + C_3 \tag{25}$$

where C_1, C_2 and C_3 are constants.

By considering:

$$dP = \frac{\partial P}{\partial r} dr + \frac{\partial P}{\partial \theta} d\theta + \frac{\partial P}{\partial z} dz \tag{26}$$

Therefore:

$$P = P_r + P_\theta + P_z + C \tag{27}$$

where P_r, P_θ and P_z are the integrated pressure equations along the r, θ and z respectively. Finally, pressure distribution is:

$$\mathrm{P} = \rho g z - \frac{9\rho\Gamma^2}{8\pi^2 r^2} - \frac{3\rho\Gamma^2}{8\pi^2\theta^2 r^2} - \frac{3\rho z^2\Gamma^2}{8\pi^2\theta^2 r^4} + \vartheta\left(\frac{7\rho\Gamma}{6\pi\theta r^2} - \frac{3\rho\Gamma}{5\pi\theta^3 r^2} - \frac{\rho\Gamma}{\pi\theta z^2} - \frac{\rho\Gamma\theta}{\pi z^2} - \frac{2\rho\Gamma z^2}{3\pi\theta r^4} - \frac{3\rho\Gamma z^2}{5\pi r^4\theta^3}\right) + \mathrm{C} \tag{28}$$

where C equals to zero in case of no vortex ($\Gamma = 0 \rightarrow P = \rho g z$).

Forced vortex region

At forced vortex region by applying Equation (2) in Equations (11)–(13), and using Equations (8)–(10), tangential, axial and radial velocity components can be written as:

$$V_\theta = \mathrm{r}\omega \tag{29}$$

$$V_z = \frac{z}{\theta}\omega \tag{30}$$

$$V_r = \frac{r}{\theta}\omega \tag{31}$$

Spiral streamlines and velocity vectors were plotted from Equations (29) to (31) in Figure 5 as well as assumptions for plotting Figure 4.

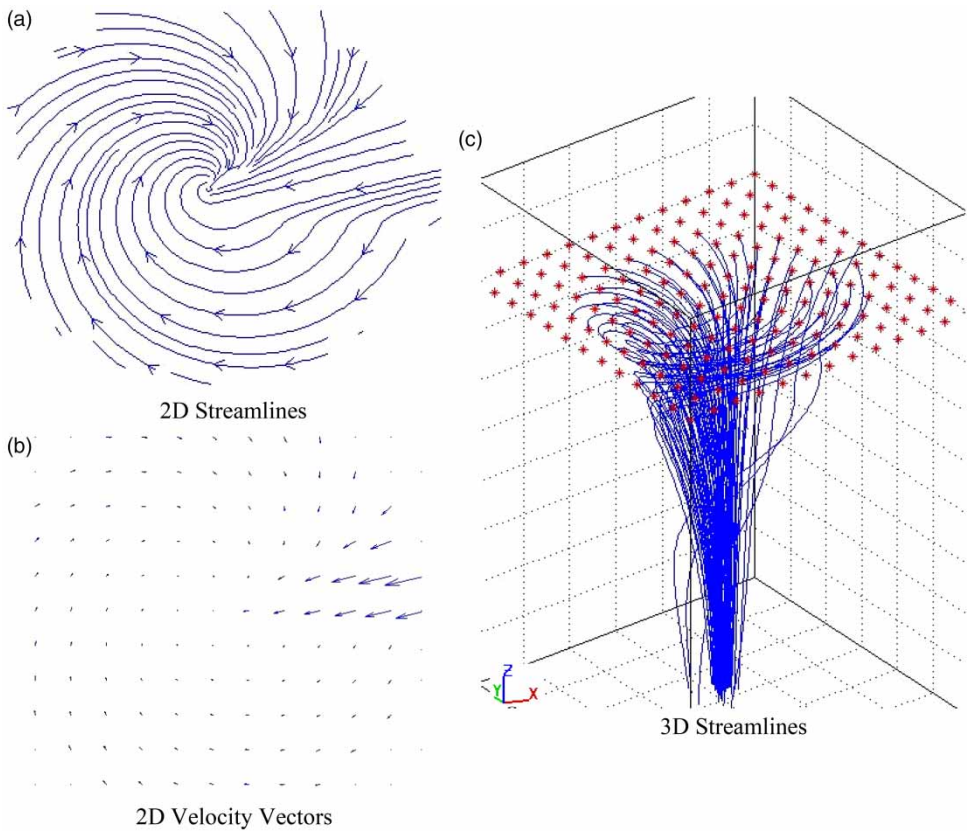

Figure 5 | Typical spiral streamlines and velocity vectors using Equations (29)–(31). (a) 2D streamlines. (b) 2D velocity vectors. (c) 3D streamlines.

Integrating Navier-Stokes equations for pressure distribution at forced vortex region:

The origin of the cylindrical coordinate system (r, z, θ) was considered at the reservoir surface, and the z-axis directed downwards (Figure 2). Substituting Equations (29)–(31) in Equations (5)–(7) and integrating them yields:

In r direction:

$$\frac{\partial P}{\partial r} = \rho r\omega^2 - \frac{3\rho\vartheta a\omega}{cr^2} \tag{32}$$

$$\mathrm{P_r} = \frac{\rho r^2\omega^2}{2} + \frac{3\rho\vartheta\omega}{\theta} + C_1 \tag{33}$$

In θ direction:

$$\frac{\partial \mathrm{P}}{\partial \theta} = -\frac{4\rho \mathrm{r} a\omega^2}{\mathrm{c}} \tag{34}$$

$$\mathrm{P_\theta} = -2\rho \mathrm{r}^2\omega^2 + C_2 \tag{35}$$

In z direction:

$$\frac{\partial \mathrm{P}}{\partial \mathrm{z}} = \rho \mathrm{g} \tag{36}$$

$$\mathrm{P_z} = \rho \mathrm{gz} + C_3 \tag{37}$$

where C_1, C_2 and C_3 are constants.

By considering:

$$dP = \frac{\partial P}{\partial r}dr + \frac{\partial P}{\partial \theta}d\theta + \frac{\partial P}{\partial z}dz \tag{38}$$

Therefore:

$$P = P_r + P_\theta + P_z + C \tag{39}$$

where P_r, P_θ and P_z are the integrated pressure equations along the r, θ and z respectively. Finally, pressure distribution is:

$$\mathrm{P} = \rho \mathrm{gz} - \frac{3\rho \mathrm{r}^2\omega^2}{2} + \frac{3\rho\vartheta\omega}{\theta} + \mathrm{C} \tag{40}$$

where C equals to zero in case of no vortex ($\omega = 0 \rightarrow P = \rho gz$).

FLUID SURFACE PROFILE

The surface profile of a vortex derived through considering P equal to zero at Equations (28) and (40) for free and forced vortex regions respectively and neglecting viscosity due to its small effect (Hite & Mih 1994):

$$a)\ \textit{Free Vortex} \rightarrow H = -\frac{4g\pi^2 + \sqrt{16g^2\pi^4 - a_1a_2}}{a_1} \qquad b)\ \textit{Forced Vortex} \rightarrow H = \frac{3r^2\omega^2}{2g} + C \tag{41}$$

where H is the water surface, C is the constant coefficient, a_1 is $3\Gamma^{-2}/\theta^2r^4$ and a_2 is $(9\theta^2\Gamma^{-2} + 3\Gamma^{-2})/\theta^2r^2$. For example in Figure 6, Equations (41)a and (41)b is plotted for $\Gamma = 0.4$, $\omega = 2.5$, $g = 9.81$, $\pi = 3.14$ and $C = -0.081$.

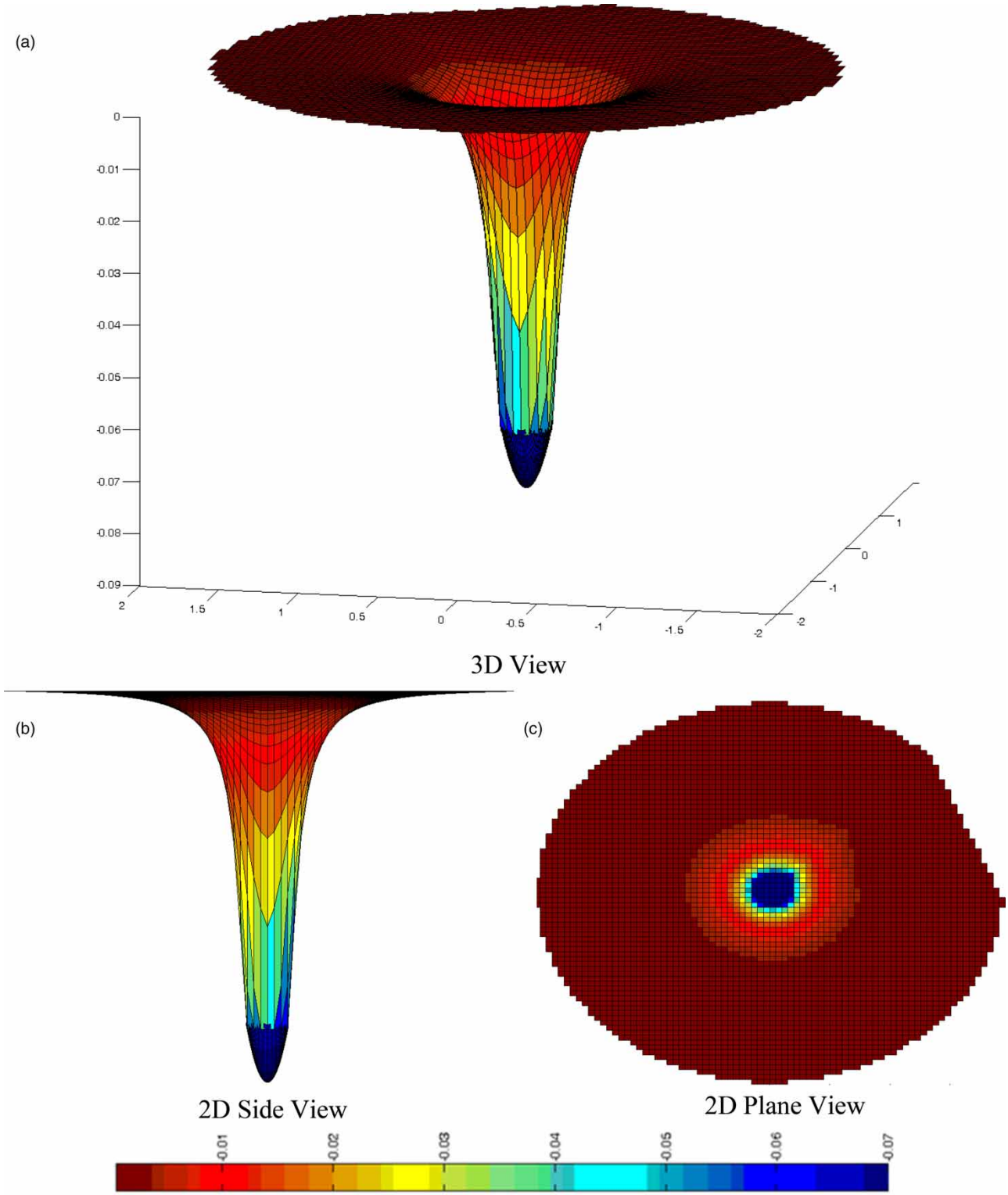

Figure 6 | Water surface profile (cm). (a) 3D view. (b) 2D side view. (c) 2D plane view.

To find the radius at the maximum tangential velocity (r_m) which demarcates the inner core and outer zone of vortex, Equations (1) and (2) was used.

$$r_m = \sqrt{\frac{\Gamma}{2\pi\omega}} \tag{42}$$

Hite & Mih (1994) proposed an equation for predicting free surface profile of a vortex:

$$H = \frac{1}{g}\left(\frac{\Gamma}{2\pi r_m}\right)^2 \frac{2\left(\frac{r}{r_m}\right)^2}{1+2\left(\frac{r}{r_m}\right)^2} + H_0 \tag{43}$$

where H_0 is the water surface elevation at the center. The result of spiral model for free surface profile was compared with Hite & Mih (1994) equation (Equation (43)) in Figure 7.

As can be seen from Figure 7, spiral model predicts water surface profile trend as same as Hite & Mih (1994) with maximum difference in water depth about 20%.

CRITICAL SUBMERGED DEPTH

To calculate critical submerged depth, a vertical intake is considered (Figure 2). When a Type 6 vortex forms at an intake and the air core reaches the intake entrance (Figure 2(a)), pressure at the intake entrance will be atmospheric (equal to zero). If such a boundary condition is used in Equation (28) the Equation (44) is derived:

$$\begin{aligned} &2160\mathrm{N}_\Gamma^2\left(\frac{\mathrm{S_c}}{\mathrm{D}}\right)^3 + 45Fr^2\left(\frac{\mathrm{S_c}}{\mathrm{D}}\right) + 180Fr^2\left(\frac{\mathrm{S_c}}{\mathrm{D}}\right)^3 = 120\left(\frac{\mathrm{S_c}}{\mathrm{D}}\right)^4 + \frac{280Fr^2}{Re}\left(\frac{\mathrm{S_c}}{\mathrm{D}}\right)^2 - \frac{9Fr^4}{Re\mathrm{N}_\Gamma^2} - \frac{60Fr^2}{Re} \\ &- \frac{960\mathrm{N}_\Gamma^2}{Re}\left(\frac{\mathrm{S_c}}{\mathrm{D}}\right)^2 - \frac{640Fr^2}{Re}\left(\frac{\mathrm{S_c}}{\mathrm{D}}\right)^4 - \frac{36Fr^4}{\mathrm{N}_\Gamma^2 Re}\left(\frac{\mathrm{S_c}}{\mathrm{D}}\right)^2 \end{aligned} \tag{44}$$

where Fr is Froude Number ($=V/g^{1/2}D^{1/2}$), Re is Reynolds Number ($=VD/\vartheta$), S/D is relative submerged depth and N_Γ is Circulation Number ($=\Gamma/2\pi g^{1/2}D^{3/2}$). If viscosity is neglected in the region of free surface vortex, Equation (44) is simplified and solved for S_c/D as:

$$\left(\frac{S_c}{D}\right)^3 - (18\mathrm{N}_\Gamma^2 + 1.5Fr^2)\left(\frac{S_c}{D}\right)^2 - 0.375Fr^2 = 0 \tag{45}$$

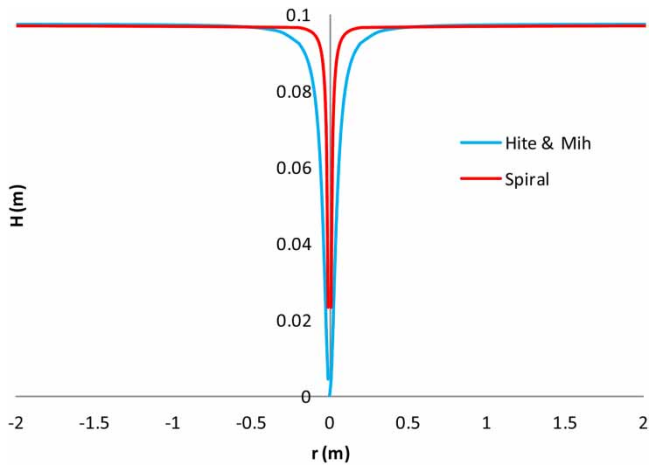

Figure 7 | Comparison of free surface profile between Spiral Model and Hite & Mih (1994).

Table 1 | Experimental data of Paul (Odgaard 1986) on an air core vortex in a vertical intake

Intake velocity V (m/s)	Intake pipe diameter D (m)	Vortex strength Γ (m^2/s)	Critical submerged depth S_c (m)
0.241	0.1528	0.3600	0.72
0.417	0.1528	0.4700	1.25
0.370	0.0663	0.1384	0.50
1.336	0.0160	0.0184	0.42
0.259	0.1017	0.2289	0.52
0.510	0.0383	0.0680	0.43
0.707	0.0288	0.0420	0.41

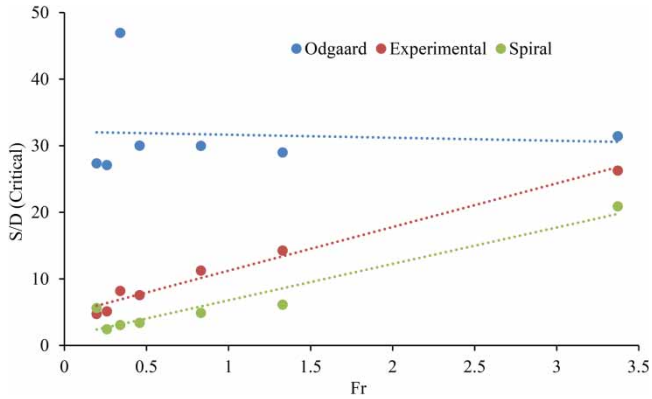

Figure 8 | Comparison between results of the present spiral model for critical submerged depth with experimental data of Paul (Odgaard 1986) and analytical model of Odgaard (1986).

Equation (45) has one real and two unreal roots and can be analytically solved for S/D. It should be noted that to calculate the critical submergence in the present analytical model, the boundary between force and free vortex region at the intake entrance was considered equal to $D/4$. To verify Equation (45), experimental results of Paul (Odgaard 1986) and analytical equation of Odgaard (1986) was utilized. Paul (Odgaard 1986) measured critical submerged depth at a vertical intake (Table 1).

The prediction of the present spiral model (Equation (45)) for critical submerged depth is compared with experimental data of Paul (Odgaard 1986) in Figure 8. Results of Odgaard (1986) equation (Equation (3)) are also shown in this figure.

As can be seen from Figure 8, Odgaard (1986) over estimated S/D with a different trend compared to the experimental data. Figure 8 shows that the results of the present analytical study are near to the experimental data and with a similar trend.

CONCLUSIONS

In the present analytical study, a spiral model for vortex flow was introduced. In this model, the spiral equations were applied in the 3D cylindrical Navier-Stokes equations. After substituting, differentiating and integrating equations, velocity and pressure distributions and also fluid surface profile were yielded. For a practical verification, an air core vortex as a critical state at intakes was selected. Water surface of an air core free surface vortex was plotted and compared with Hite & Mih (1994) proposed equation and the deviation was found to be about 20% in the maximum point. Using the present spiral model, an equation for critical submerged depth was derived and compared with experimental data of Paul (Odgaard 1986) and analytical equation of Odgaard (1986). Results showed that present spiral model could predict $(S/D)_{cr}$ in good agreement with experimental data.

DATA AVAILABILITY STATEMENT

All relevant data are included in the paper or its Supplementary Information.

REFERENCES

Amiri, S. M., Zarrati, A. R., Roshan, R. & Sarkardeh, H. 2011 Surface vortex prevention at power intakes by horizontal plates. *J. Water Manage. (ICE)* **164** (4), 193–200.

Amphlett, M. B. 1976 *Air-entraining Vortices at A Horizontal Intake*. Rep. No.OD/7. HRS, Wallingford, UK.

Andersen, A., Bohr, T., Stenum, B., Rasmussen, J. J. & Lautrup, B. 2003 Anatomy of a bathtub vortex. *Phys. Rev. Lett.* **91**, 104502.

Andersen, A., Bohr, T., Stenum, B., Rasmussen, J. J. & Lautrup, B. 2006 The bathtub vortex in a rotating container. *J. Fluid Mech.* **556**, 121–146.

Anwar, H. O., Weller, J. A. & Amphlett, M. B. 1978 Similarity of free vortex at horizontal intake. *J. Hydraul. Res.* **16** (2), 95–105.

Berge, J. P. 1966 A study of vortex formation and other abnormal flow in a tank with and without a free surface. *La Houille Blancher*. **52** (1), 13–40.

Chang, E. 1977 *Review of Literature on Drain Vortices in Cylindrical Tanks*. Rep. No. TN. 1342, British Hydromechanics Research Association (BHRA), Bedford, UK.

Constantinescu, G. S. & Patel, V. C. 1998 Numerical model for simulation of pump-intake flow and vortices. *J. Hydraul. Eng.* **124** (2), 123–134.

Constantinescu, G. S. & Patel, V. C. 2000 Role of turbulence model in prediction of pump-bay vortices. *J. Hydraul. Eng.* **126** (5), 387–391.

Denny, D. F. & Young, G. H. J. 1957 The prevention of vortices and swirl at intakes. In: *Proc. of 7th IAHR Congress*, Vol. 1. International Association for Hydro-Environmental Engineering and Research (IAHR), Lisbon, pp. C1-1–C1-18.

Gordon, J. L. 1970 Vortices at intakes structures. *Water Power* **22** (4), 137–138.

Hite, J. E. & Mih, W. 1994 Velocity of air-core vortices at hydraulic intakes. *ASCE J. Hydraul Eng.* **120** (3), 284–297.

Jain, A. K., Raju, K. G. R. & Garde, R. J. 1978 Vortex formation at vertical pipe intake. *J. Hydraul. Div.* **104** (10), 1429–1445.

Khadem Rabe, B., Ghoreishi Najafabadi, S. H. & Sarkardeh, H. 2018 Numerical simulation of anti-vortex devices at water intakes. *Proc. Inst. Civ. Eng. Water Manag.* **171** (1), 18–29.

Khanarmuei, M. R., Rahimzadeh, H., Kakuei, A. R. & Sarkardeh, H. 2016 Effect of vortex formation on sediment transport at dual pipe intakes. *Sādhanā* **41**, 1055–1061.

Knauss, J. 1987 *Swirling Flow Problems at Intakes*. Hydraulic Struc. Design Manual, Balkema, the Netherlands.

Lautrup, B. 2005 *Physics of Continuous Matter: Exotic and Everyday Phenomena in the Macroscopic World*. IoP Publishing, Bristol, UK.

Li, W. H. & Lam, S. H. 1964 *Principles of Fluid Mechanics*. Addison Wesley, Boston, MA.

Lucino, C., Liscia, S. & Duró, G. 2010 Vortex detection in pump sumps by means of CFD. In *XXIV Latin American Congress Hydraulics Punta Del Este*, Uruguay.

Lugt, H. J. 1983 *Vortex Flow in Nature and Technology*. J. Wiley Hoboken, NJ.

Lundgren, T. S. 1985 The vertical flow above the drain-hole in a rotating vessel. *J. Fluid Mech.* **155**, 381–412.

Marghzar, S. H., Montazerin, N. & Rahimzadeh, H. 2003 Flow field, turbulence and critical condition at a horizontal water intake. *Proc. Inst. Mech. Eng. A* **217** (1), 53–62.

Miles, J. 1998 A note on the Burgers–Rott vortex with a free surface. *Z. Angew. Math. Phys.* **49**, 162–165.

Odgaard, A. J. 1986 Free-surface air core vortex. *J. Hydraul. Engng ASCE* **112**, 610–620.

Padmanabhan, M. & Hecker, G. E. 1984 Scale effects in pump sump models. *J. Hydraulic Eng.* **110** (11), 1540–1556.

Pakdel, E., Majdzadeh Tabatabai, M. R., Sarkardeh, H. & Ghoreishi Najafabadi, S. H. 2020 Elimination of vortices by wave generation as a hydraulic anti-vortex method. *J Braz. Soc. Mech. Sci. Eng.* **42**, 571.

Panagopoulos, A. 2021 Water-energy nexus: desalination technologies and renewable energy sources. *Environ. Sci. Pollut. Res.* 1–14.

Panagopoulos, A. & Haralambous, K. J. 2020 Minimal liquid discharge (MLD) and zero liquid discharge (ZLD) strategies for wastewater management and resource recovery - analysis, challenges and prospects. *J. Environ. Chem. Eng.* **8** (5), 104418.

Panagopoulos, A., Haralambous, K. J. & Loizidou, M. 2019 Desalination brine disposal methods and treatment technologies - a review. *Sci. Total Environ.* **693**, 133545.

Rankine, W. J. M. 1858 *Manual of Applied Mechanics*. C. Griffen Co., London, England.

Reddy, Y. R. & Pickford, J. A. 1972 Vortices at intakes in conventional sumps. *Water Power* **24** (3), 108–109.

Roshan, R., Sarkardeh, H. & Zarrati, A. R. 2009 Vortex study on a hydraulic model of Godar-e-Landar dam and hydropower plant. *WIT Trans. Eng. Sci.* **63**, 217–225.

Rott, N. 1958 On the viscous core of a line vortex. *Z. Angew Math. Phys.* **9b**, 543–553.

Sarkardeh, H., Zarrati, A. R. & Roshan, R. 2010 Effect of intake head wall and trash rack on vortices. *J. Hydraul. Res.* **48** (1), 108–112.

Sarkardeh, H., Zarrati, A. R., Jabbari, E. & Roshan, R. 2012 Discussion of prediction of intake vortex risk by nearest neighbors modeling. *ASCE J. Hydraul. Eng.* **137** (6), 701–705.

Sarkardeh, H., Jabbari, E., Zarrati, A. R. & Tavakkol, S. 2013 Velocity field in a reservoir in the presence of an air-core vortex. *J. Water Management (ICE)* **164** (4), 193–200.

Sarkardeh, H., Zarrati, A. R., Jabbari, E. & Marosi, M. 2014 Numerical simulation and analysis of flow in a reservoir in the presence of vortex. *Eng. Appl. Comput. Fluid Mech.* **8** (4), 598–608.

Schneider, A., Conrad, D. & Bohle, M. 2015 Lattice Boltzmann simulation of the flow field in pump intakes – a new approach. *J. Fluids Eng.* **137** (3), 031105.

Shukla, S. N. & Kshirsagar, J. T. 2008 Numerical Prediction of Air Entrainment in Pump Intakes. In: *Proceedings of the Twenty-Fourth International Pump Users Symposium*.

Stepanyants, Y. A. & Yeoh, G. H. 2008 Stationary bathtub vortices and a critical regime of liquid discharge. *J. Fluid Mech.* **604**, 77–98.

Tahershamsi, A., Rahimzadeh, H., Monshizadeh, M. & Sarkardeh, H. 2018 An experimental study on free surface vortex dynamics. *Meccanica* **53**, 3269–3277.

White, F. M. 2003 *Fluid Mechanics*, 5th edn. McGraw-Hill, New York, NY.

WRI 1992 *Karun I Power Intakes Model Studies*. Hydraulic Structures Division, Iran.

Yildirim, N., Eyüpoğlu, A. & Taştan, K. 2012 Critical submergence for dual rectangular intakes. *ASCE J. Energy Eng.* **138** (4), 237–245.

First received 29 March 2021; accepted in revised form 17 August 2021. Available online 31 August 2021